

Measurement of the transverse polarization of electrons emitted in neutron decay – nTRV experiment

K. Bodek^{1*} and A. Kozela²

¹ M. Smoluchowski Institute of Physics, Jagiellonian University, Cracow, Poland

² H. Niewodniczański Institute of Nuclear Physics, Polish Academy of Sciences, Cracow, Poland

* kazimierz.bodek@uj.edu.pl

March 22, 2021



Review of Particle Physics at PSI
doi:[10.21468/SciPostPhysProc.2](https://doi.org/10.21468/SciPostPhysProc.2)

Abstract

The two components of the transverse polarization of electrons (σ_{T_1} , σ_{T_2}) emitted in the β -decay of polarized, free neutrons have been measured. The T-odd, P-odd correlation coefficient, R , quantifying σ_{T_2} , perpendicular to the neutron polarization and electron momentum, was found to be $0.004 \pm 0.012 \pm 0.005$. This value is consistent with time-reversal invariance, and significantly improves limits on the relative strength of imaginary scalar couplings in the weak interaction. The value obtained for the correlation coefficient N , $0.067 \pm 0.011 \pm 0.004$, associated with σ_{T_1} , agrees with the Standard Model expectation, providing an important sensitivity test of the experimental setup.

15.1 Introduction

Nuclear and neutron beta decay have played a central role in the development of the weak interaction theory. Among the empirical foundations of the electroweak Standard Model (SM), the assumptions of maximal parity violation, the vector and axial-vector character, and massless neutrinos are directly linked to nuclear and neutron beta decay experiments. Beta decay theory was firmly established about four decades ago and became a part of the SM. It describes the semi-leptonic and strangeness-conserving processes in the 1-st particle generation mediated by charged W -boson exchange. More recently, the neutrino masses have been shown to be finite – beta decay experiments with increasing precision still confirm the first two assumptions. Despite the great success of the SM, many open questions remain such as the origin of parity violation, the hierarchy of fermion masses, the number of particle generations, the mechanism of CP violation, and the unexplained large number of parameters of the theory. A discovery of new CP- or T-violating phenomena, especially in systems built of light quarks, with vanishingly small contributions of CKM matrix induced mechanism, different from those reported for heavier systems in [1, 2], would be a major breakthrough. Nuclear beta decay experiments study the light-quark systems and free neutron decay plays a particularly important role. It is free of complications connected with nuclear and atomic structure due to its simplicity. In addition, final state interaction effects, which can mimic T violation, are minimal and can be calculated with a relative precision better than 1% [3–5].

The nTRV project at PSI, was the first experimental search for the real and imaginary parts of the scalar and tensor couplings using the measurement of the transverse polarization of electrons emitted in the free neutron decay. There are very few measurements of this observable in general [6, 7], and only two in nuclear beta decays. One of them, for the ^8Li system [8], provides the most stringent limit on the tensor coupling constants of the weak interaction.

43 According to [9], the decay rate distribution from polarized neutrons as a function of elec-
44 tron energy (E) and momentum (\mathbf{p}) is proportional to:

$$\omega(\mathbf{J}, \hat{\boldsymbol{\sigma}}, E, \mathbf{p}) \propto 1 + \frac{\langle \mathbf{J} \rangle}{J} \cdot \left(A \frac{\mathbf{p}}{E} + R \frac{\mathbf{p} \times \hat{\boldsymbol{\sigma}}}{E} + N \hat{\boldsymbol{\sigma}} \right) + \dots \quad (15.1)$$

45 where $\frac{\langle \mathbf{J} \rangle}{J}$ ($J = |\mathbf{J}|$) is the neutron polarization, $\hat{\boldsymbol{\sigma}}$ is the unit vector onto which the electron spin
46 is projected, and A is the beta decay asymmetry parameter. N and R are correlation coefficients
47 which, for neutron decay with usual SM assumptions: $C_V = C'_V = 1$, $C_A = C'_A = \lambda = -1.276$ [10]
48 and allowing for a small admixture of scalar and tensor couplings C_S , C_T , C'_S , C'_T , can be
49 expressed as:

$$N = -0.218 \cdot \text{Re}(\mathfrak{S}) + 0.335 \cdot \text{Re}(\mathfrak{T}) - \frac{m}{E} \cdot A, \quad (15.2)$$

$$R = -0.218 \cdot \text{Im}(\mathfrak{S}) + 0.335 \cdot \text{Im}(\mathfrak{T}) - \frac{m}{137p} \cdot A, \quad (15.3)$$

50 where $\mathfrak{S} \equiv (C_S + C'_S)/C_V$, $\mathfrak{T} \equiv (C_T + C'_T)/C_A$ and m is the electron mass. The R correlation coef-
51 ficient vanishes in the lowest order SM calculations. It becomes finite if final state interactions
52 are included, $R_{FSI} \approx -\frac{m}{137p} \cdot A \approx 0.0006$, below the sensitivity of this experiment. A larger
53 value of R would provide evidence for the existence of exotic couplings, and a new source
54 of time reversal violation (TRV). Using Mott polarimetry, both transverse components of the
55 electron polarization can be measured simultaneously: σ_{T_2} perpendicular to the decay plane
56 defined by the neutron spin and electron momentum associated with R , and σ_{T_1} contained in
57 the decay plane and associated with N . The SM value of N is finite and well within reach of
58 this experiment. Its determination provides an important test of the experimental sensitivity.

59 15.2 Experiment

60 The experiment was performed at the FUNSPIN beam line [11] at the neutron source SINQ of
61 the Paul Scherrer Institute, Villigen, Switzerland. A detailed description of the design, oper-
62 ation and performance of the Mott polarimeter can be found in [12]. Only a short overview
63 is presented here. The final result comprises independent analyses of four data collection peri-
64 ods, featuring different basic conditions such as beam polarization, Mott foil thickness and
65 acquired statistics.

66 The Mott polarimeter consisted of two identical modules, arranged symmetrically on either
67 side of the neutron beam (Figure 15.1). The whole structure was mounted inside a large-
68 volume dipole magnet providing a homogeneous vertical spin-holding field of 0.5 mT within
69 the beam fiducial volume. An RF-spin flipper (not shown in Figure 15.1) was used to reverse
70 the orientation of the neutron beam polarization at regular time intervals, typically every 16 s.
71 Going outwards from the beam, each module consisted of a multi-wire proportional chamber
72 (MWPC) for electron tracking, a removable Mott scatterer (1-2 μm Pb layer evaporated on a
73 2.5 μm thick mylar foil) and a scintillator hodoscope to measure the electron energy.

74 A 1-cm-thick plastic scintillator, used for the electron energy reconstruction, had a reso-
75 lution of 33 keV at 500 keV. The asymmetry of the light signal collected at the ends of the
76 scintillator slab was used to determine the vertical hit position with a resolution of about 6
77 cm: the segmentation (10 cm) of the hodoscope in the horizontal direction provided a crude
78 estimate of the z-coordinate. Matching the information from the precise track reconstruction
79 in the MWPC with that from the scintillator hodoscope reduced background and random co-
80 incidences considerably.

81 A 1.3-m-long multi-slit collimator defined the beam cross section to $4 \times 16 \text{ cm}^2$ at the en-
82 trance of the Mott polarimeter. To minimize neutron scattering and capture, the entire beam
83 volume, from the collimator to the beam dump, was enclosed in a chamber lined with ${}^6\text{Li}$

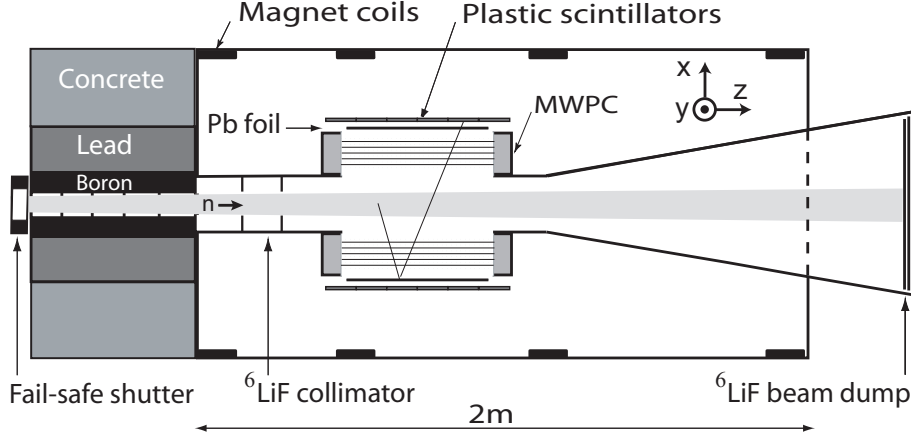


Figure 15.1: Schematic top view of the experimental setup. A sample projection of an electron V-track event is indicated.

84 polymer and filled with pure helium at atmospheric pressure. The total flux of the collimated
 85 beam was typically about 10^{10} neutrons/sec. Thorough investigations of the beam polarization
 86 performed in a dedicated experiment [11] showed a substantial dependence on the position
 87 in the beam fiducial volume. The average beam polarization necessary for the evaluation of
 88 the N - and R -correlation coefficients was extracted from the observed decay asymmetry using
 89 the precisely known [10] beta decay asymmetry parameter $A = -0.1196 \pm 0.0002$. This ap-
 90 proach automatically accounts for the proper integration over the position-dependent beam
 91 density, its polarization and detector acceptance. For this purpose, single track events (only
 92 one reconstructed track segment on the hit scintillator side) were recorded using a dedicated
 93 prescaled trigger. The main event trigger was used to find V-track candidates: events with two
 94 reconstructed segments on one side and one segment accompanied by a scintillator hit on the
 95 opposite side, (see Figure 15.1).

96 The following asymmetries were analyzed to extract the beam polarization, P :

$$\mathcal{E}(\beta, \gamma) = \frac{N^+(\beta, \gamma) - N^-(\beta, \gamma)}{N^+(\beta, \gamma) + N^-(\beta, \gamma)} = P\beta A \cos(\gamma), \quad (15.4)$$

97 where N^\pm are experimental, background-corrected counts of single tracks sorted in 4 bins of
 98 the electron velocity β , and 15 bins of the electron emission angle γ with respect to the neutron
 99 polarization direction. The sign in the superscripts reflects the beam polarization direction.

100 A comparison between the measured and MC simulated energy spectra for direct and Mott-
 101 scattered electrons is shown in Figure 15.2 a and b, respectively. Electronic thresholds are not
 102 included in the simulation – this is why the measured and simulated distributions do not match
 103 at the low energy side.

104 Another set of asymmetries was used to extract the N and R correlation coefficients :

$$\mathcal{A}(\alpha) = \frac{n^+(\alpha) - n^-(\alpha)}{n^+(\alpha) + n^-(\alpha)}, \quad (15.5)$$

105 where n^\pm represent background-corrected experimental numbers of counts of V-track events,
 106 sorted in 12 bins of α , the angle between electron scattering and neutron decay planes. In
 107 the case of V-track events, beside the background discussed previously, events for which the
 108 scattering took place in the surrounding of the Mott-target provide an additional source of
 109 background. Figure 15.2 c shows the distribution of the reconstructed vertex positions in the
 110 x -direction for data collected with and without the Mott foil. The distribution clearly peaks at
 111 the foil position. The “foil-out” distribution has been scaled appropriately by a factor deduced
 112 from the accumulated neutron beam.

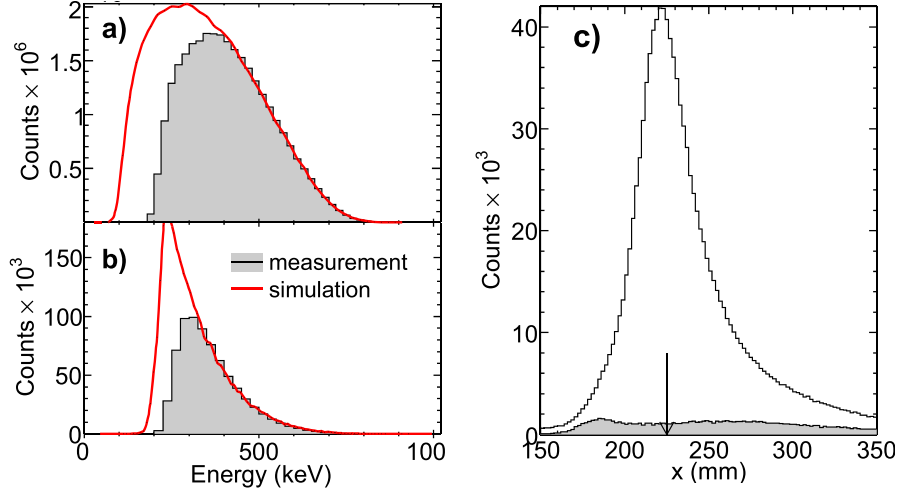


Figure 15.2: Background-corrected experimental energy distributions (shaded areas) of (a) the single-track and (b) V-track events compared with simulations. (c) Background contribution (shaded) to vertex x -coordinate distribution of V-track events. The arrow indicates the Mott foil position.

113 It can be shown [12] that

$$A(\alpha) - P\bar{\beta}A\bar{F}(\alpha) = P\bar{S}(\alpha) [N\bar{G}(\alpha) + R\bar{\beta}\bar{H}(\alpha)], \quad (15.6)$$

114 where the kinematical factors $\bar{F}(\alpha)$, $\bar{G}(\alpha)$, and $\bar{H}(\alpha)$ represent the average values of the quan-
 115 tities $\hat{\mathbf{J}} \cdot \hat{\mathbf{p}}$, $\hat{\mathbf{J}} \cdot \hat{\boldsymbol{\sigma}}$ and $\hat{\mathbf{J}} \cdot \hat{\mathbf{p}} \times \hat{\boldsymbol{\sigma}}$, respectively, \bar{S} is the effective analyzing power of the electron
 116 Mott scattering, known in the literature as ‘‘Sherman function’’, and the bar over a letter indi-
 117 cates event-by-event averaging. The term $P\bar{\beta}A\bar{F}$ accounts for the β -decay-asymmetry-induced
 118 nonuniform illumination of the Mott foil. Since the $\bar{\beta}$ and \bar{F} are known precisely from event-
 119 by-event averaging, the uncertainty of this term is dominated by the error of the average beam
 120 polarization P .

121 Mean values of the effective analyzing powers as a function of electron energy, scattering
 122 and incidence angles were calculated using the Geant 4 simulation framework [13], following
 123 guidelines presented in [14, 15]. This approach accounts properly for the atomic structure,
 124 nuclear size effects as well as the effects introduced by multiple scattering in thick foils.

125 The systematic uncertainty is dominated by the effects introduced by the background sub-
 126 traction procedure, connected with the choice of the geometrical cuts defining event classes
 127 ‘‘from-beam’’ and ‘‘off-beam’’. To estimate this effect, the cuts were varied in a range limited
 128 solely by the geometry of the apparatus. Because the radio-frequency of the spin flippers
 129 was a small source of noise in the readout electronics, tiny spin-flipper-correlated dead time
 130 variations were observed. The result was corrected for this effect.

131 The asymmetries as defined in (15.4) and (15.5) have been calculated for events with
 132 energies above the neutron β -decay end-point energy and for events originating outside of
 133 the beam fiducial volume: they were found to be consistent with zero within the statistical
 134 accuracy, which proves that the data were not biased e.g. with a spin-flipper-related false
 135 asymmetry.

136 A fit of the experimental asymmetries \mathcal{A} , corrected for the $P\bar{\beta}A\bar{F}$ term for the experimental
 137 data set of 2007 is shown in Figure 15.3.

138 From the approximate symmetry of the detector with respect to the transformation $\alpha \rightarrow -\alpha$,
 139 it follows that $\bar{\beta}$, \bar{S} and the factors \bar{F} , \bar{H} are all symmetric, while \bar{G} is an antisymmetric function

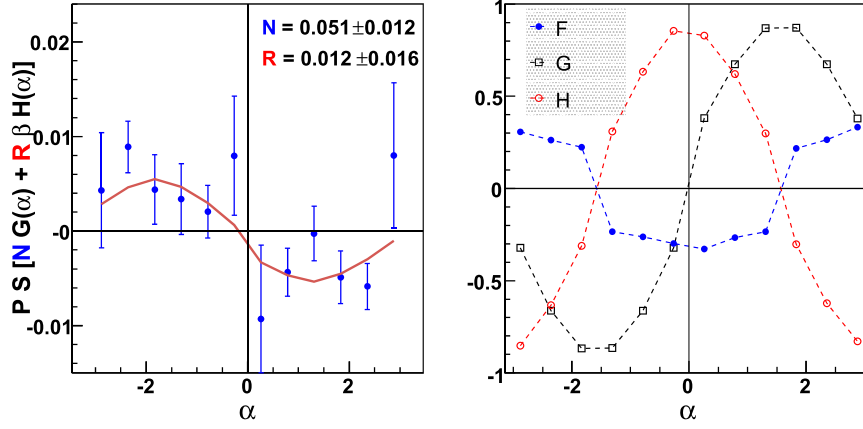


Figure 15.3: Left panel: experimental asymmetries \mathcal{A} corrected for the $P\bar{\beta}A\bar{F}$ term for the 2007 data set as a function of α (defined in text). The solid line illustrates a two-parameter (N, R) least-square fit to the data. The indicated errors are statistical. Right panel: geometrical factors $\bar{F}(\alpha)$, $\bar{G}(\alpha)$ and $\bar{H}(\alpha)$ for the same data set

140 of α (see Figure 15.3). This allows the extraction of the N coefficient from the expression [12]:

141

$$N \approx \frac{(r-1)}{(r+1)} \cdot \frac{1 - \frac{1}{2}(P\bar{\beta}A\bar{F})^2}{P\bar{S}\bar{G}}, \quad r = \sqrt{\frac{n^+(\alpha)n^-(-\alpha)}{n^-(\alpha)n^+(-\alpha)}} \quad (15.7)$$

142 The advantage of this method is that the effect connected with the term $P\bar{\beta}A\bar{F}$ is suppressed by
 143 a factor of about 60 compared to (15.6). The good agreement between the N values obtained
 144 in both ways enhances confidence in the extracted N and R coefficient values.

145 The systematic uncertainties in the evaluation of the R and N coefficients are dominated by
 146 effects introduced by the background subtraction procedure and the choice of specific values
 147 of the cuts that determine whether an individual event is attributed to “signal” or to “back-
 148 ground”. These effects were systematically studied for all data sets. Additional calibration
 149 measurements were performed to determine the Mott-target mass distribution [16] that can
 150 influence the electron depolarization leading to increased uncertainty of the effective Sherman
 151 function. A detailed description of the data analysis process can be found in [17, 18] together
 152 with the final result comprising all available experimental data.

$$R = 0.004 \pm 0.012_{\text{stat}} \pm 0.005_{\text{syst}}, \quad (15.8)$$

$$N = 0.067 \pm 0.022_{\text{stat}} \pm 0.004_{\text{syst}}. \quad (15.9)$$

153 This was the first determination of the N correlation coefficient in β -decay.

154 In Figure 15.4 the new results are included in exclusion plots containing all experimental
 155 information available from nuclear and neutron beta decays as surveyed in [19]. The upper
 156 plots contain the normalized scalar and tensor coupling constants \mathfrak{S} and \mathfrak{T} , while the lower
 157 plots correspond to the helicity projection amplitudes in the leptoquark exchange model, as
 158 defined in [20]. Although the achieved accuracy does not improve the already strong con-
 159 straints on the real part of the couplings (left panels), the result is consistent with the existing
 160 data and increases confidence in the validity of the extraction of R . For the imaginary part
 161 (right panels), the new experimental value of the R coefficient significantly constrains scalar
 162 couplings beyond the limits from all previous measurements. The result is consistent with the
 163 SM.

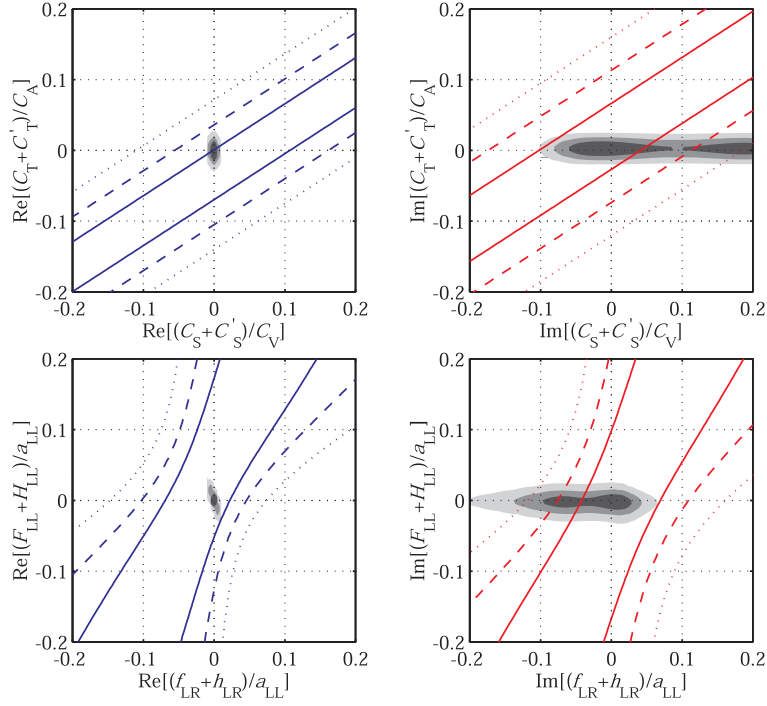


Figure 15.4: Experimental bounds on the scalar vs. tensor normalized couplings (upper) and leptokuark exchange helicity projection amplitudes (lower panels). The gray areas represent the information as defined in [19], while the lines represent the limits resulting from the present experiment. Solid, dashed and dotted lines correspond to 1-, 2- and 3- sigma confidence levels, respectively, in analogy to decreasing intensity of the grey areas.

15.3 Outlook – the BRAND project

The successful determination of two transverse components of the polarization of electrons emitted in neutron decay in a pioneering and nearly optimal experiment led to the following conclusions: (i) it seems quite possible to decrease the systematic uncertainty by an order of magnitude using existing techniques, (ii) the transverse electron polarization can be studied in a more systematic way by correlating it with the electron momentum, the neutron spin, and also with the recoil proton momentum by constructing larger and higher acceptance detecting systems like e.g. proposed by [21] and operating with the highest intensity polarized cold neutron beam available. In this way, one can study seven correlation coefficients: H , L , N , R , S , U and V where five of them (H , L , S , U , V) have never been experimentally studied:

$$\begin{aligned}
 \omega(E_e, \Omega_e, \Omega_{\bar{\nu}}) &\propto 1 + \\
 &a \frac{\mathbf{p}_e \cdot \mathbf{p}_{\bar{\nu}}}{E_e E_{\bar{\nu}}} + b \frac{m_e}{E_e} + \frac{\langle \mathbf{J} \rangle}{J} \cdot \left[A \frac{\mathbf{p}_e}{E_e} + B \frac{\mathbf{p}_{\bar{\nu}}}{E_{\bar{\nu}}} + D \frac{\mathbf{p}_e \times \mathbf{p}_{\bar{\nu}}}{E_e E_{\bar{\nu}}} \right] + \\
 &\sigma_{\perp} \cdot \left[H \frac{\mathbf{p}_{\bar{\nu}}}{E_{\bar{\nu}}} + L \frac{\mathbf{p}_e \times \mathbf{p}_{\bar{\nu}}}{E_e E_{\bar{\nu}}} + N \frac{\langle \mathbf{J} \rangle}{J} + R \frac{\langle \mathbf{J} \rangle \times \mathbf{p}_e}{J E_e} + \right. \\
 &\left. S \frac{\langle \mathbf{J} \rangle \mathbf{p}_e \cdot \mathbf{p}_{\bar{\nu}}}{J E_e E_{\bar{\nu}}} + U \mathbf{p}_{\bar{\nu}} \frac{\langle \mathbf{J} \rangle \cdot \mathbf{p}_e}{J E_e E_{\bar{\nu}}} + V \frac{\mathbf{p}_{\bar{\nu}} \times \langle \mathbf{J} \rangle}{J E_{\bar{\nu}}} \right], \tag{15.10}
 \end{aligned}$$

where σ_{\perp} represents a unit vector perpendicular to the electron momentum \mathbf{p}_e and $J = |\mathbf{J}|$. $\mathbf{p}_{\bar{\nu}}$ and $E_{\bar{\nu}}$ are the antineutrino momentum and energy, respectively.

The coefficients relating the transverse electron polarization to \mathbf{p}_e , $\mathbf{p}_{\bar{\nu}}$ and \mathbf{J} have several interesting features. They vanish for the SM weak interaction, and reveal the variable size

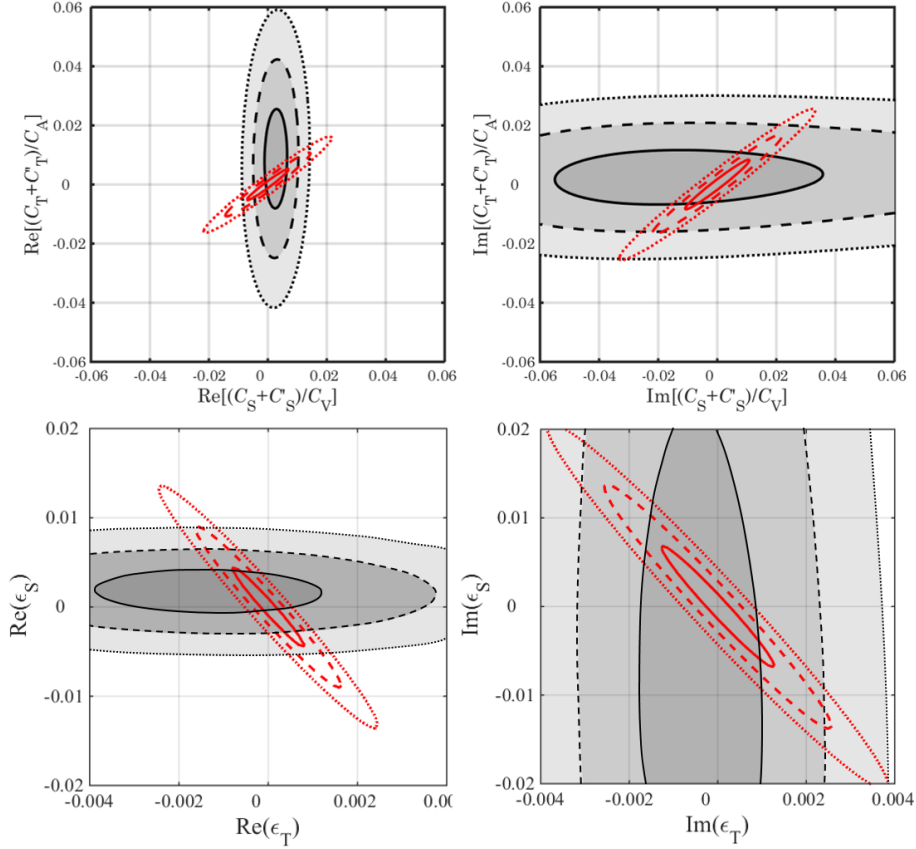


Figure 15.5: Experimental bounds on the scalar vs. tensor couplings \mathfrak{S} , \mathfrak{T} from (15.2) (upper panels) and translated to EFT parameters ϵ_S , ϵ_T (lower panels). The gray areas represent the information deduced from presently available experiments, while the red lines represent the limits resulting from the correlation coefficients H , L , N , R , S , U and V measured with the anticipated accuracy of 5×10^{-4} . Solid, dashed and dotted lines correspond to 1-, 2- and 3- σ confidence levels, respectively, in analogy to decreasing intensity of the grey areas.

178 of the electromagnetic contributions. For H and N , the electromagnetic contributions are of
 179 the order of 0.06, which can be used for an internal sensitivity check of the Mott polarimeter.
 180 Finally, the dependence on the real and imaginary parts of the scalar and tensor couplings
 181 alternates exclusively from one correlation coefficient to another with varying sensitivity. This
 182 feature allows a complete set of constraints to be determined from the neutron decay alone.

183 The idea of implementing such a complex measurement was proposed in [22]. An updated
 184 version of the measurement can be found in [23]. Presently, the first test run devoted to the
 185 verification of the applied detectors and techniques has been completed on the PF1B cold
 186 neutron beam at the Laue Langevin Institute in Grenoble, France (ILL).

187 15.4 EFT parameterization

188 To bridge the classical β -decay formalism with high-energy physics and permit sensitivity com-
 189 parison of low-energy charged-current observables with measurements carried out at high-
 190 energy colliders, the model-independent effective field theory (EFT) framework is employed.
 191 The effective nucleon-level couplings C_i , C'_i ($i \in [V, A, S, T]$) can be generally expressed as
 192 combinations of the quark-level parameters ϵ_i , $\tilde{\epsilon}_i$ ($i \in [L, R, S, T]$) [24]. The imaginary parts
 193 of the scalar and tensor couplings parameterize CP-violating contributions. The high energy

194 BSM physics process that can be compared with β -decay experiments is the cross section for
195 electrons and missing transverse energy (MET) in $pp \rightarrow e\bar{\nu} + MET + \dots$ channel since it has
196 the same underlying partonic process as in β -decay ($\bar{u}d \rightarrow e\bar{\nu}$). With the anticipated accuracy
197 of about 5×10^{-4} for the transverse electron polarization related correlation coefficients one
198 would obtain significantly tighter bounds on the real and imaginary parts of scalar and tensor
199 coupling constants and, consequently, on ϵ_S and ϵ_T as shown in Figure 15.5. It should be
200 noted that such limits would be competitive to those extracted from the analysis of 20 fb^{-1}
201 CMS collaboration data collected at 8 TeV [25, 26] and even to the planned measurements at
202 14 TeV.

203 Acknowledgments

204 This work has been supported in part by The National Science Centre, Poland, under the grant
205 No. 2018/29/B/ST2/02505.

206 References

- 207 [1] J. H. Christenson *et al.*, *Evidence for the 2π decay of the K_2^0 meson*, Phys. Rev. Lett. **13**,
208 138 (1964).
- 209 [2] K. Abe *et al.*, *Improved measurement of mixing-induced CP violation in the neutral B meson*
210 *system*, Phys. Rev. D **66**, 071102 (2002).
- 211 [3] P. Vogel and B. Werner, *Final-state interactions and time-reversal tests in nuclear β -decay*,
212 Nuclear Physics A **404**, 345 (1983).
- 213 [4] A. N. Ivanov *et al.*, *Test of the Standard Model in Neutron Beta Decay with Polarized Electron*
214 *and Unpolarized Neutron and Proton*, Phys. Rev. D **99**, 053004 (2019).
- 215 [5] A. N. Ivanov *et al.*, *Corrections of order $O(E_e^2/m_N^2)$, caused by weak magnetism and pro-*
216 *ton recoil, to the neutron lifetime and correlation coefficients of the neutron beta decay*,
217 arXiv:2010.14336 [hep-ph] (2020).
- 218 [6] N. Danneberg *et al.*, *Muon Decay: Measurement of the Transverse Polarization of the Decay*
219 *Positrons and its Implications for the Fermi Coupling Constant and Time Reversal Invariance*,
220 Phys. Rev. Lett. **94**, 021802 (2005).
- 221 [7] M. Abe *et al.*, *New Limit on the T-Violating Transverse Muon Polarization in $K^+ \rightarrow \pi^0 \mu^+ \nu$*
222 *Decays*, Phys. Rev. Lett. **93**, 131601 (2004).
- 223 [8] R. Huber *et al.*, *Search for Time-Reversal Violation in the β Decay of Polarized ^8Li Nuclei*,
224 Phys. Rev. Lett. **90**, 202301 (2003).
- 225 [9] J. D. Jackson *et al.*, *Possible Tests of Time Reversal Invariance in Beta Decay*, Phys. Rev.
226 **106**, 517 (1957).
- 227 [10] P. A. Zyla *et al.*, *Particle Data Group*, Prog. Theor. Exp. Phys. **2020**, 083C01 (2020).
- 228 [11] J. Zejma *et al.*, *FUNSPIN polarized cold-neutron beam at PSI*, Nucl. Instr. Meth. Phys. Res.,
229 Sect. A **539**, 622 (2005).
- 230 [12] G. Ban *et al.*, *A Mott polarimeter for the search of time reversal violation in the decay of free*
231 *neutrons*, Nucl. Instrum. Meth. A **565**, 711 (2006), doi:[10.1016/j.nima.2006.05.166](https://doi.org/10.1016/j.nima.2006.05.166).

- 232 [13] S. Agostinelli *et al.*, *Geant4 – a simulation toolkit*, Nucl. Instr. Meth. Phys. Res., Sect. A
233 **506**, 250 (2003).
- 234 [14] F. Salvat *et al.*, *ELSEPA – Dirac partial-wave calculation of elastic scattering of electrons and*
235 *positrons by atoms, positive ions and molecules*, Comp. Phys. Comm. **165**, 157 (2005).
- 236 [15] M. A. Khakoo *et al.*, *Monte Carlo studies of Mott scattering asymmetries from gold foils*,
237 Phys. Rev. D **64**, 052713 (2001).
- 238 [16] A. Kozela *et al.*, *Thickness scan of metallic layer by photon induced X-ray emission*, Nucl.
239 Instr. Meth. in Phys. Res., Sect. B **269**, 1767 (2010).
- 240 [17] A. Kozela *et al.*, *Measurement of the transverse polarization of electrons emitted in free*
241 *neutron decay*, Phys. Rev. Lett. **102**, 172301 (2009).
- 242 [18] A. Kozela *et al.*, *Measurement of the transverse polarization of electrons emitted in free*
243 *neutron decay*, Phys. Rev. C. **85**, 045501 (2012).
- 244 [19] N. Severijns *et al.*, *Tests of the standard electroweak model in beta decay*, Rev. Mod. Phys.,
245 Sect. A **78**, 991 (2006).
- 246 [20] P. Herczeg, *Beta decay beyond the standard model*, Prog. Part. Nucl. Phys. **46**, 413 (2001).
- 247 [21] J. Sromicki, *T Violation in the weak scalar and tensor interaction: neutron and nuclei*,
248 Nucl. Instr. Meth. in Phys. Res., Sect. A **440**, 609 (2000).
- 249 [22] K. Bodek, *R- and N-correlation coefficients in neutron decay: Search for scalar and tensor*
250 *couplings in weak interactions*, Physics Procedia **17**, 30 (2011).
- 251 [23] K. Bodek *et al.*, *BRAND: Search for BSM physics at TeV scale by exploring transverse po-*
252 *larization of electrons emitted in neutron decay*, EPJ Web of Conferences **219**, 04001
253 (2018).
- 254 [24] O. Naviliat-Cuncic *et al.*, *Prospects for precision measurements in nuclear β decay in the*
255 *LHC era*, Ann. Phys. **525**, 600 (2013).
- 256 [25] S. Chatrchyan and others (CMS Collaboration), *Search for new physics in events with*
257 *same-sign dileptons and b-tagged jets in pp collisions at $s = 7$ TeV*, JHEP **1208**, 023 (2012).
- 258 [26] V. Khachatryan and others (CMS Collaboration), *Search for physics beyond the standard*
259 *model in final states with a lepton and missing transverse energy in proton-proton collisions*
260 *at $s = 8$ TeV*, Phys. Rev. D **91**, 092005 (2015).